



## OPEN ACCESS

## EDITED BY

Robert W. Góra,  
Wrocław University of Science and Technology,  
Poland

## REVIEWED BY

Yanping Liu,  
Zhejiang Ocean University, China  
Zakir Hussain,  
University of Baltistan, Pakistan

## \*CORRESPONDENCE

Haihua Xu,  
✉ xuhaihua2024@163.com  
Waris Khan,  
✉ wariskhan758@yahoo.com

RECEIVED 12 July 2024

ACCEPTED 30 September 2024

PUBLISHED 14 January 2025

## CITATION

Xu H, Awwad FA, Ismail EAA and Khan W (2025) Mathematical model and stability of SWCNT- and MWCNT-based nanofluid flow with thermal and chemically reactive effects inside a porous vertical cone.

*Front. Chem.* 12:1463778.

doi: 10.3389/fchem.2024.1463778

## COPYRIGHT

© 2025 Xu, Awwad, Ismail and Khan. This is an open-access article distributed under the terms of the [Creative Commons Attribution License \(CC BY\)](https://creativecommons.org/licenses/by/4.0/). The use, distribution or reproduction in other forums is permitted, provided the original author(s) and the copyright owner(s) are credited and that the original publication in this journal is cited, in accordance with accepted academic practice. No use, distribution or reproduction is permitted which does not comply with these terms.

# Mathematical model and stability of SWCNT- and MWCNT-based nanofluid flow with thermal and chemically reactive effects inside a porous vertical cone

Haihua Xu<sup>1\*</sup>, Fuad A. Awwad<sup>2</sup>, Emad A. A. Ismail<sup>2</sup> and Waris Khan<sup>3\*</sup>

<sup>1</sup>School of Mechanical Engineering, Chongqing Three Gorges University, Chongqing, China,

<sup>2</sup>Department of Quantitative Analysis, College of Business Administration, King Saud University, Riyadh, Saudi Arabia, <sup>3</sup>Department of Mathematics and Statistics, Hazara University, Mansehra, Pakistan

This study investigates the significance of single-walled (SWCNTs) and multi-walled (MWCNTs) carbon nanotubes with a convective fluid (water) over a vertical cone under the influences of chemical reaction, magnetic field, thermal radiation and saturated porous media. The impact of heat sources is also examined. Based on the flow assumptions, the fundamental flow equations are modeled as partial differential equations (PDEs). Using the appropriate transformation, the PDEs are converted to ordinary differential equations and then solved via RK4 in MATLAB. To confirm the results, a comparison is made with a previously investigated problem, finding good agreement. The emerging dimensionless physical parameters impact on the flow problem is determined through graphs and tables. Analysis reveals a dual solution for the suction and injection parameter. Therefore, stability examination is implemented to confirm a stable solution. The aim of the study is to analyze SWCNTs and MWCNTs in a vertical cone with stability to establish that only the first solution is reliable. The analysis here signifies that large volume fractions can be substituted to increase the nanofluid movement. The mathematical model and graphical demonstration indicate that the velocity of MWCNTs is higher than SWCNTs. Moreover, the local skin friction, rate of heat transfer, and Nusselt and Sherwood numbers improve with Biot number.

## KEYWORDS

numerical investigation, dual solution, stability analysis, nanofluid, thermal radiation, solutal boundary layer, chemical performance, heat source

## 1 Introduction

Heat transmission is crucial for both machine performance and material choice. The biological sciences, thermoregulation, bio-heat transfer activities, and blood circulation all greatly benefit from heat transmission. Every biological and mechanical process eventually loses efficiency because it generates heat; regular heat removal from a system is required to maximize its effectiveness. Nanofluids (NFs) are novel substances which can regulate heat conduction. Water, polymerization, engine oil, and various lubricants are examples of common fluids that have lower heating conductivity than solids. Increasing the heat conductivity of such fluids is as simple as adding a certain quantity of solid particles.

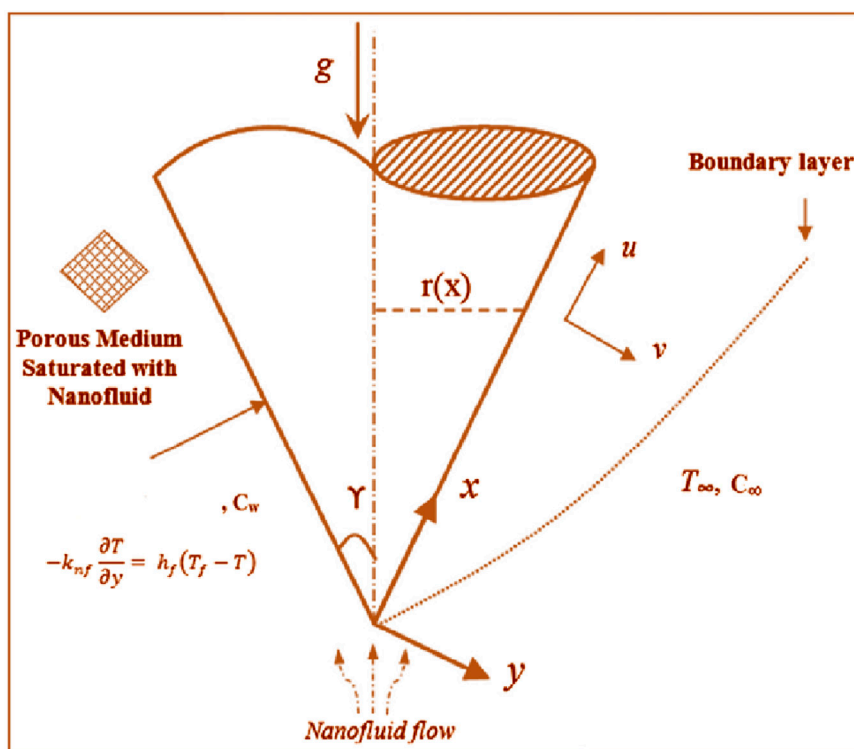


FIGURE 1 Flow geometry.

Nanomaterials are small particles, typically 1–100 nm in size; their resulting fluid is known as “nanofluid”. Choi and Eastman (1995a; 1995b) first recommended the creation of NFs. Xuan and Li (2000) discussed developments in NF heat transmission. To analyze the movement of NFs, Buongiorno (2006) derived a model that included thermophoresis and Brownian motion dynamics. Many singularities, including the reduction or augmentation of the network’s thermal magnitude, the buildup of microchannels, the miniaturization of the entire structure, and minimum clogging, may be better understood using NFs. The electromagnetic dipole impact on Williamson NF under heat was studied by Khan et al. (2020a); they also investigated entropy production on magneto-fluid under robin restrictions with dissipation (Khan et al., 2020b).

Memon et al. (2022) and Abu-Bakr et al. (2022) discuss the larger body of work on heat transmission using NFs. Because of its extensive uses in industry, research, and engineering, heat-mass transfer has attracted much scholarly attention. It is crucial for raising the threshold for final product quality and finds use in ferromagnetic medication targeting and the cooling process of electronic gadgets, among other chemical and pharmacological processes. Hayat et al. (2017a) studied the computational analysis of carbon nanotubes (CNTs) with slip conditions. Hayat et al. (2017b) investigated homogeneous as well as heterogeneous influences in fluid movement with joule heating. Hussain et al. (2022) reported the slip and joule effects in NF over stretched plate. Similarly, Hayat et al. (2019) examined Jeffrey NF in Darcian flow with heat source and melting effects. Other practical uses include insulation, the storage of thermal energy, the extraction and utilization of fossil fuels, the paper sector, food preparation, the

TABLE 1 Thermo-properties of nanofluid.

Fluid	$\rho$ ( $\frac{kg}{m^3}$ )	$C_p$ ( $\frac{J}{kgK}$ )	$k$ ( $\frac{W}{mk}$ )
Base fluid	997.1	4,179	0.613
SWCNTs	2,600	425	6,600
MWCNTs	1,600	796	3,000

inclusion of oxygen, drying porous solids, dialysis treatment, underground energy dissemination, and the restoration of geothermal energy. Peristaltic movement, heat transmission, mass transportation, and chemical processes were all investigated by HinanS et al. (2012).

CNTs have malleable strengths ranging 11–63 GPa and an ultra-high Young’s modulus of roughly 1 TPa—extraordinary mechanical qualities. The elimination of heat is currently of importance to the electronics sector as it strives to achieve higher levels of degenerative power. In order to create future generations of ICs and 3D technological devices, we must determine which materials offer the best heat transfer properties. A CNT is a man-made cylinder made from a rolled-up strip of graphene that can be either a single- or multi-well structure. CNTs with only one hole and a diameter of 0.4–3 nm are called “single-wall carbon nanotubes” (SWCNTs), whereas CNTs with multiple wells and a diameter of 0.4–30 nm are called “multi-wall carbon nanotubes” (MWCNTs). CNTs are employed in a wide variety of industries, including water purification, healthcare, nanotechnology battery production, superconductivity, electronics, recycling, transplantation, solar

energy storage, and biological sensors. Using Maxwell hypothesis, Xue (2005) provided a model for thermal conduction that shows the effect of space-dispersed CNTs in a spinning tube. When the liquid heat is 25°C, the heating capacity of the CNTs-based nanofluid is enhanced by up to 30%; at 40°C, the augmentation rises to 79%. Khan (2023a) used ferro nanoparticles to examine the agnetized Williamson NF. The unsteady thermal mass transfer unmagnetized Sutterby NF was studied by Azeem Khan (2022). The radioactive impact in Eyring–Powell fluid comprising gyrotactic microorganisms was described by Khan (2023b). A computational approach was developed for thermally Eyring–Powell fluid exposed to biological convection behavior (Anjum et al., 2022). Waqas et al. (2022) studied the ferromagnetic Casson NF that comprises stratifications in bio-convection movement.

The heat transmission rates of MWCNTs suspended in filtered water across a horizontal heated tube were experimentally investigated by Amrollahi et al. (2010); for a nanotube volume fraction of 0.25%, they found a 33–40% increase in the laminar heat transmission coefficient. The thermal properties of convectonal (water) CNT NF was experimentally established to be improved by 100%–250% by Rashmi et al. (2011). Thermophysical characteristics and the general efficacy of MWCNT oil-depending NF movement across helically wrapped tubes was reported by Pakdamana et al. (2012), who also noted an increase in thermal efficiency when the volume friction of suspended CNTs was 0.1%, 0.2%, or 0.4%. Heat transmission along with pressure drop of CNT-convectonal (water) NF through a flat cylindrical tube using distilled water as base fluid was inspected by Wang et al. (2013). Using several types of nanoparticles, Akbar et al. (2023a) investigated the peristaltic motion of magnetized tiny fluids. The heat transfer of a magnetized elastic liquid through entropy impact was studied by Akbar et al. (2023b). Using a non-uniform structure, Maraj et al. (2023) investigated NF in peristaltic mobility. Similarly, Akbar et al. (2024) examined thermal properties in microchannels using copper and silver nanotechnology in micropolar liquid. The heat phenomenon in Eyring–Powell fluid across an extensible sheet was observed by Alghamdi et al. (2024).

The fields of biomedical science, optics, magnetic cell segregation, silk float separations, nonlinear optics, heat exhaustion, drug administration, and optical grates are a few applications of magnetic NFs, in which liquid and magnetic characteristics coexist. There has been much research into movement and heat mass transportation using magnetic NFs (Hayat et al., 2011; Chamkha and Rashad, 2014; Sudarsana Reddy and Chamkha, 2016a; Sudarsana Reddy and Chamkha, 2016b; Tasawar et al., 2015). Heatline analysis was provided by Khan et al. (2015) to investigate heat transportation using inclined heated surface containing CuO-water-based NF. Numerical analysis conducted by Selimefendigil and Oztop (2016a) on Al<sub>2</sub>O<sub>3</sub> and CuO-water-based NF in an vertical heated cavity found that heat transportation upsurges with the volume fraction of nano-size particles. Magnetized mixed conduction heat exchange improvement of CuO-based NF over a lid-driven chamber was studied by Selimefendigil and Oztop (2016b), who discovered that the absolute magnitude of average heat transmission rises from 1 to 100 when the Richardson number grows. Heat transmission was shown to decrease with increasing Hartman number in natural porous

chamber flow containing CuO NF (Miroshnichenko et al., 2016; Oztop et al., 2017).

According to Amrollahi et al. (2010), Rashmi et al. (2011), Pakdamana et al. (2012), Wang et al. (2013), and Akbar et al. (2023a), there is no research on the inspiration of radiation effect on the SWCNT and MWCNT NF flowing in an upward cone via porous media with heat source and convective boundary conditions enclosing heat mass transportation with stability analysis. This study aims to investigate the significance of SWCNTs and MWCNTs in convectonal fluid (water) over a vertical cone under the influences of chemical reaction, magnetism, thermal radiation, and drenched porous media. The impact of heat is also examined. Based on the flow molds, the fundamental flow characteristics are modeled in term of partial differential equations (PDEs). Using the appropriate transformation, the PDEs are dimentionalized in terms of conventional derivatives (ordinary differential equations) and then solved via RK4 in MATLAB. The present analysis reveals the dual solution for the suction and injection parameter. Therefore, an immovability investigation is conducted to confirm which solution is stable. This study is analyzes SWCNTs and MWCNTs in vertical cones with stability to establish that only the first solution is reliable. Solar systems, refinement systems, pharmaceutical materials, and thermal electrodes are the immediate applications of this analysis.

## 2 Mathematical analysis

Laminar flow is studied in two dimensions across a porous vertical cone containing single and multiple CNTs based on an aqueous nanofluid movement with anomalous thermal performance (Figure 1). Table 1 demonstrates the thermophysical features of the base fluid (water) and CNTs. The x-axis of the selected geometry coincides with the path of flow through the cone’s surface. The unknown temperature  $T_w$  is due to convective warming process with properties such as the initial temperature  $T_f$  and the heat transfer coefficient  $h_f$ , where  $\phi_w$  is the NVF at the cone’s surface,  $T_\infty$  is the heat of the ambient fluid, and  $\phi_\infty$  is the NVF of the ambient fluid. The y-axis is subject to the magnetic field.

The leading flow equations in the occurrence of chemical, suction, injection, radiation, porous matrix, and heat mass transfer are described in Equations 1–6 by, Amrollahi et al. (2010), Rashmi et al. (2011), Pakdamana et al. (2012), Wang et al. (2013), and Akbar et al. (2023a):

$$\frac{\partial(ru)}{\partial x} + \frac{\partial(rv)}{\partial y} = 0, \tag{1}$$

$$u \frac{\partial u}{\partial x} + v \frac{\partial u}{\partial y} = \frac{\mu_{nf}}{\rho_{nf}} \frac{\partial^2 u}{\partial y^2} - \frac{\mu_{nf}}{\rho_{nf}} \frac{1}{K} u + g[\beta(T - T_\infty) - \beta^*(\phi - \phi_\infty)] \cos \gamma - \frac{\sigma B_0^2}{\rho_{nf}} u, \tag{2}$$

$$u \frac{\partial T}{\partial x} + v \frac{\partial T}{\partial y} = \alpha_{nf} \frac{\partial^2 T}{\partial y^2} - \frac{1}{(\rho c_p)_{nf}} \frac{\partial q_r}{\partial y}, \tag{3}$$

$$u \frac{\partial \phi}{\partial x} + v \frac{\partial \phi}{\partial y} = D_m \frac{\partial^2 \phi}{\partial y^2} - K_r(\phi - \phi_\infty), \tag{4}$$

with boundary conditions

$$u = 0, v = V_1(x), -k_{nf} \frac{\partial T}{\partial y} = h_f(T_f - T), \phi = \phi_w \text{ at } y = 0, \quad (5)$$

$$u \rightarrow 0, T \rightarrow T_\infty, \phi \rightarrow \phi_\infty \text{ at } y \rightarrow \infty, \quad (6)$$

$$q_r = -\frac{16T_\infty^3 \sigma^*}{3K^*} \frac{\partial T}{\partial y}. \quad (7)$$

Here,  $u$  and  $v$  signify the velocity components alongside the coordinate axes  $x$  and  $y$ , respectively. The expression  $V_0 = \frac{3a}{4x} Ra_x^{1/4} v_1$  denotes the mass transportation along the surface with suction ( $v_1 < 0$ ) and injection ( $v_1 > 0$ ).

The thermal boundary conditions applied to a surface or contact in a system where convection is the primary mode of heat transmission are known as “convective boundary conditions”. The movement of a fluid and a solid surface to transfer heat is the main concern in setting a convective boundary condition. A common description of convective heat transport at a boundary is provided by Newton’s law of cooling.

Here,  $T^4$  is expressed in terms of a Taylor sequence as follows:

$$T^4 = T_\infty^4 + 4T_\infty^3(T - T_\infty) + 6T_\infty^2(T - T_\infty)^2 + \dots$$

Neglecting higher-order terms, we derive

$$T^4 \cong 4T_\infty^3 T - 3T_\infty^4. \quad (8)$$

By substituting Equation 8 in Equation 7, We get, Equation 9,

$$q_r = -\frac{16T_\infty^3 \sigma^*}{3K^*} \frac{\partial T}{\partial y}. \quad (9)$$

Thermal conductivity  $k_{nf}$  is expressed as follows:

$$\mu_{nf} = \frac{\mu_f}{(1 - \phi)^{2.5}}, \rho_{nf} = (1 - \phi)\rho_f + \rho_{CNT}\phi, \alpha_{nf} = \frac{k_{nf}}{(\rho c_p)_{nf}},$$

$$(\rho c_p)_{nf} = (1 - \phi)(\rho c_p)_f + \phi(\rho c_p)_{CNT},$$

$$k_{nf} = k_f \left( \frac{(1 - \phi) + 2\phi \left( \frac{k_{CNT}}{k_{CNT} - k_f} \right) \ln \left( \frac{k_{CNT} + k_f}{2k_f} \right)}{(1 - \phi) + 2\phi \left( \frac{k_f}{k_{CNT} - k_f} \right) \ln \left( \frac{k_{CNT} + k_f}{2k_f} \right)} \right).$$

Introducing the similarity transformations:

$$\eta = \frac{y}{x} Ra_x^{1/4}, f(\eta) = \frac{\psi}{\alpha Ra_x^{1/4}}, \theta(\eta) = \frac{T - T_\infty}{T_w - T_\infty}, S(\eta) = \frac{\phi - \phi_\infty}{\phi_w - \phi_\infty}, \quad (10)$$

where  $Ra_x$  is the local Rayleigh number and is defined as

$$Ra_x = \frac{g\beta_{bf}\rho_{bf}(T - T_\infty)x^3 \cos \gamma}{\mu_{bf}\alpha_{bf}}$$

$$f''' + \frac{A_1}{Pr} \left[ \frac{3}{4} f f'' - \frac{1}{2} (f')^2 \right] - k_1 f' - \frac{A_1}{A_2} M f' + A_1 [\theta - NrS] = 0, \quad (11)$$

$$(1 + R)\theta'' + \frac{3}{4} A_3 A_4 f \theta' = 0, \quad (12)$$

$$S'' + \frac{3}{4} Sc f S' - Cr.S = 0. \quad (13)$$

The corresponding boundary constraints are

$$\eta = 0, f = V_0, f' = 0, \theta'(0) = -A_4 B_1 (1 - \theta(0)), S = 1. \quad (14)$$

$$\eta \rightarrow \infty, f' = 0, \theta = 0, S = 0.$$

TABLE 2 Confirmation of the present study by comparison of  $f'''(0)$  with Amrollahi et al. (2010) taking water as the base fluid when  $Nr = 0, Pr = 6.2, V_0 = 0, B_1 = 0, \gamma = 0, R = 0, Cr = 0, M = 0, K_1 = 0$ .

$\phi$	$f'''(0)$			
	Khan et al. (Amrollahi et al., 2010)		Current work	
	SW-CNTs	MW-CNTs	SW-CNTs	MW-CNTs
0.1	0.33894	0.33727	0.33712	0.33736
0.2	0.40811	0.39008	0.40821	0.39001
0.3	0.50452	0.46466	0.50458	0.46344

Prime signifies a derivative with respect to  $\eta$ , and the parameters defined in the above equations are

$$Nr = \frac{\beta^*(\phi_w - \phi_\infty)}{\beta(T_w - T_\infty)}, k_1 = \frac{x^2}{K Ra_x^{1/2}}, Cr = \frac{K_r x^2}{D_m Ra_x^{1/2}}, Pr = \frac{\mu_f}{\alpha \rho_f},$$

$$R = \frac{16T_\infty^3 \sigma^*}{3K^* k_{nf}}, M = \frac{\sigma \beta_o^2 x^2}{\mu_f Ra_x^{1/2}}, Sc = \frac{\alpha}{D_m},$$

$$A_1 = (1 - \phi)^{2.5} \left[ (1 - \phi) + \phi \left( \frac{\rho_{CNT}}{\rho_f} \right) \right], B_1 = \frac{h_f x}{k_f Ra_x^{1/4}},$$

$$A_2 = (1 - \phi) + \phi \left( \frac{\rho_{CNT}}{\rho_f} \right), A_3 = (1 - \phi) + \phi \left( \frac{(\rho c_p)_{CNT}}{(\rho c_p)_f} \right),$$

$$A_4 = \frac{k_f}{k_{nf}}.$$

The physical quantities of interests are Equation 15,

$$C_f = \frac{\tau_w}{\rho U_\infty^2}, Nu_x = \frac{x q_w}{k(T_w - T_\infty)}, Sh_x = \frac{x J_w}{D_B(\phi_w - \phi_\infty)}. \quad (15)$$

### 3 RK4 solution and validation

The numerical solution was obtained for the modeled mathematical problem (17)–(20) via fourth-order Runge–Kutta (RK4). The first order ordinary differential equations are obtained in dimensionless form by using the new variables. The boundary conditions are transformed as well. The Prandtl number is fixed as 6.2 for the water, as the model is water-based SWCNTs and MWCNTs. The value of NVF varies 0.1–0.3 ( $0 < \phi \leq 0.3$ ). For conformation, the present study was related to previous analysis, and good correspondence was recognized by comparing the values of the skin friction (Table 2). This validation confirmed that the numerical fallout of the existing research is definite.

### 4 Stability analysis

We are here interested in obtaining the second solution for the various values of  $\lambda$ . For this determination, it is important to determine the immovability examination of the problem which is reliable as well as actually realistic. The method approved is by Merkin (1986) as improved by Weidman et al. (2006). The unsteady flow equations are Equation 16,

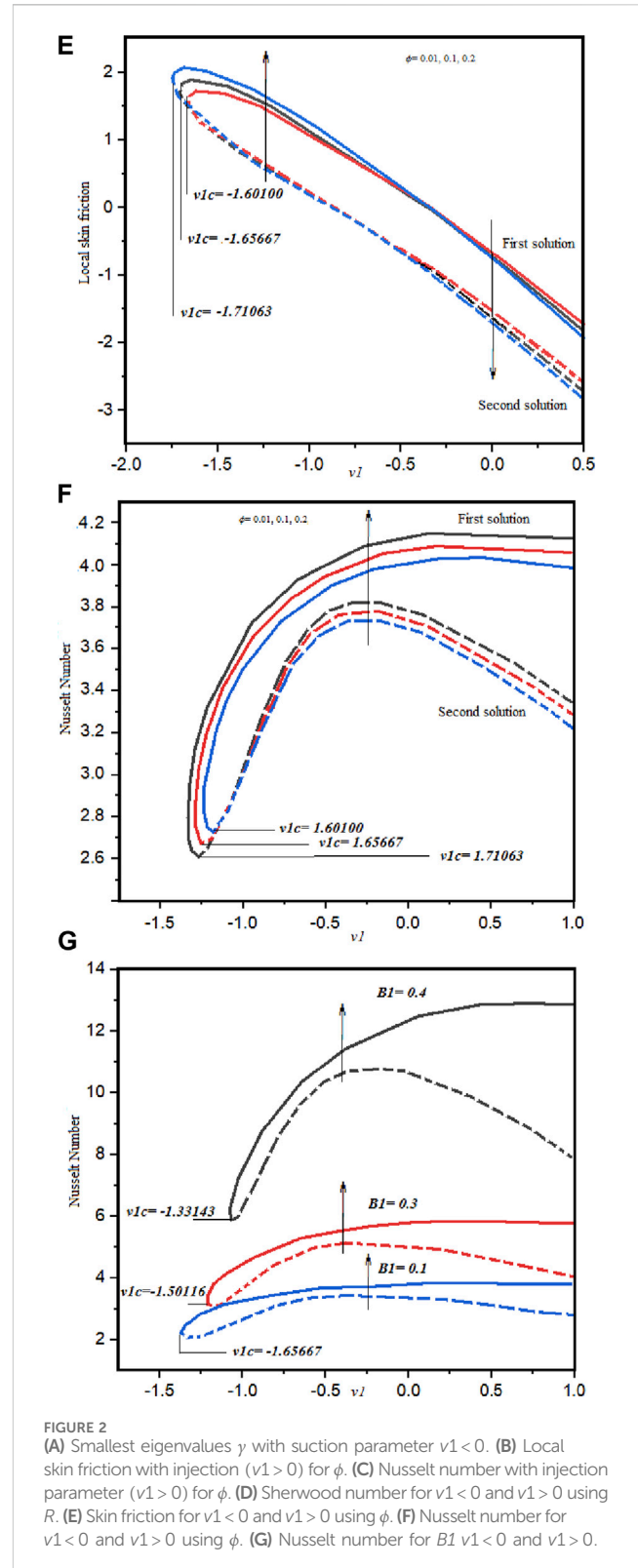
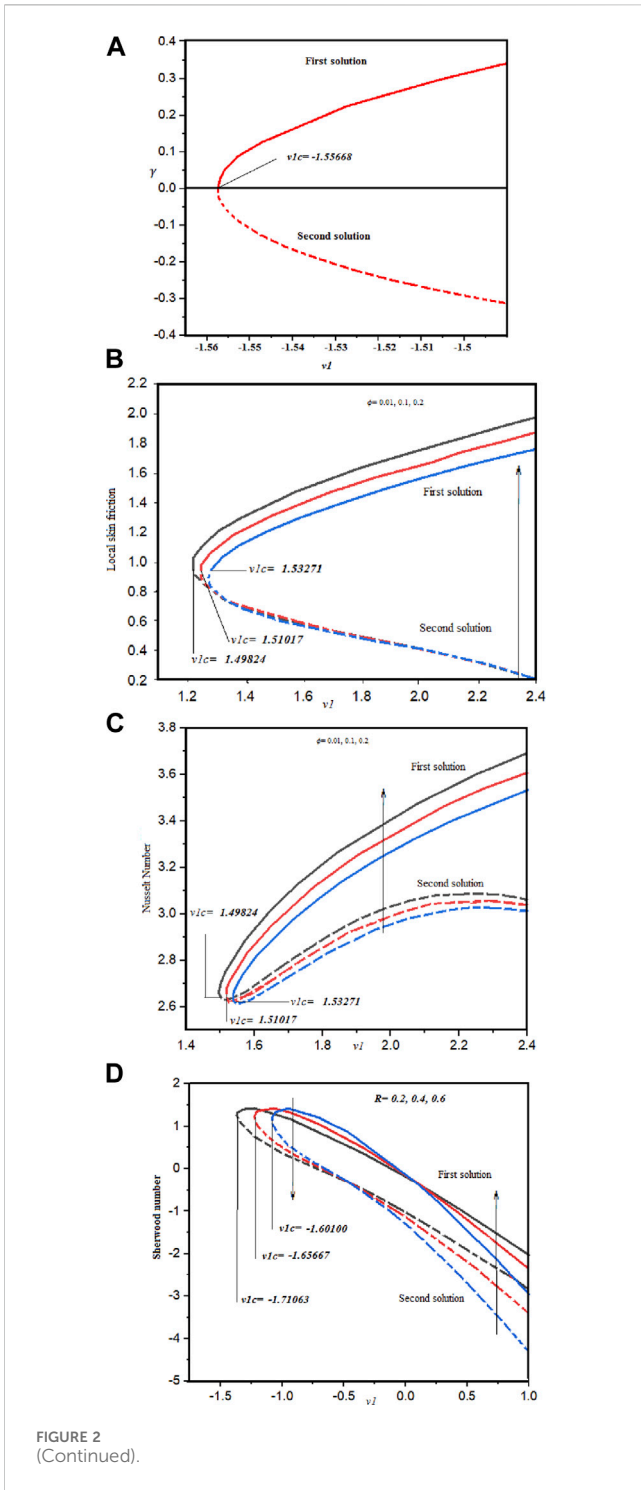


FIGURE 2 (Continued).

FIGURE 2 (A) Smallest eigenvalues  $\gamma$  with suction parameter  $v_1 < 0$ . (B) Local skin friction with injection ( $v_1 > 0$ ) for  $\phi$ . (C) Nusselt number with injection parameter ( $v_1 > 0$ ) for  $\phi$ . (D) Sherwood number for  $v_1 < 0$  and  $v_1 > 0$  using  $R$ . (E) Skin friction for  $v_1 < 0$  and  $v_1 > 0$  using  $\phi$ . (F) Nusselt number for  $v_1 < 0$  and  $v_1 > 0$  using  $\phi$ . (G) Nusselt number for  $BI$   $v_1 < 0$  and  $v_1 > 0$ .

$$\frac{\partial(ru)}{\partial x} + \frac{\partial(rv)}{\partial y} = 0, \tag{16}$$

$$\begin{aligned} \frac{\partial u}{\partial t} + u \frac{\partial u}{\partial x} + v \frac{\partial u}{\partial y} &= \frac{\mu_{nf}}{\rho_{nf}} \frac{\partial^2 u}{\partial y^2} - \frac{\mu_{nf}}{\rho_{nf}} \frac{1}{K} u \\ &+ g[\beta(T - T_{\infty}) - \beta^*(\phi - \phi_{\infty})] \cos \gamma - \frac{\sigma B_0^2}{\rho_{nf}} u, \end{aligned} \tag{17}$$

$$\frac{\partial T}{\partial t} + u \frac{\partial T}{\partial x} + v \frac{\partial T}{\partial y} = \alpha_{nf} \frac{\partial^2 T}{\partial y^2} - \frac{1}{(\rho c_p)_{nf}} \frac{\partial q_r}{\partial y}, \tag{18}$$

$$u \frac{\partial \phi}{\partial t} + \frac{\partial \phi}{\partial x} + v \frac{\partial \phi}{\partial y} = D_m \frac{\partial^2 \phi}{\partial y^2} - K_r(\phi - \phi_{\infty}), \tag{19}$$



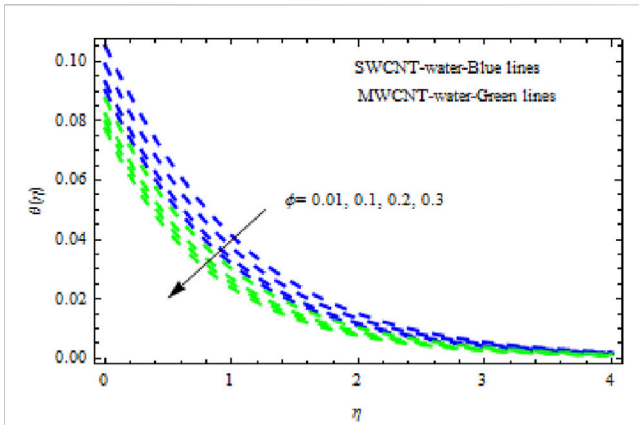


FIGURE 3 Impact of  $\phi$  on  $f'(\eta)$ .

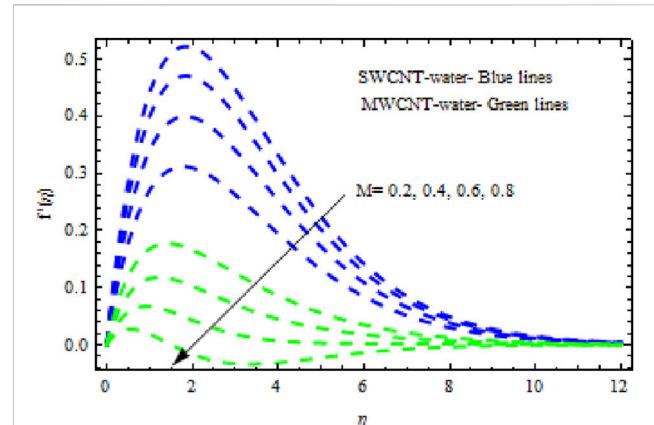


FIGURE 6 Impact of  $M$  on  $f'(\eta)$ .

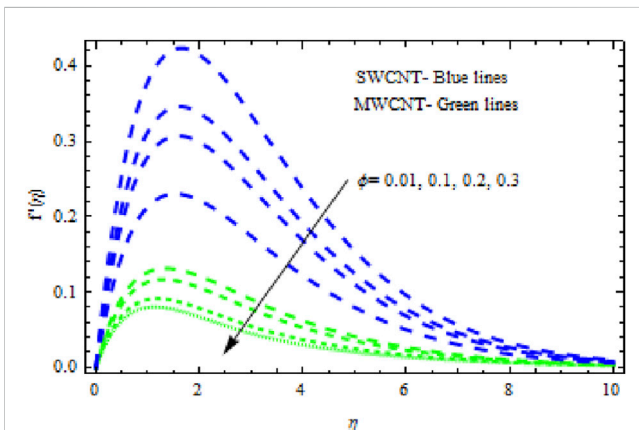


FIGURE 4 Impact of  $\phi$  on  $\theta(\eta)$ .

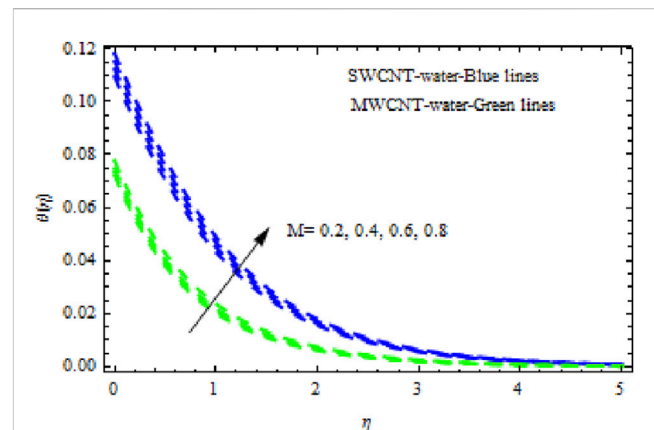


FIGURE 7 Impact of  $M$  on  $\theta(\eta)$ .

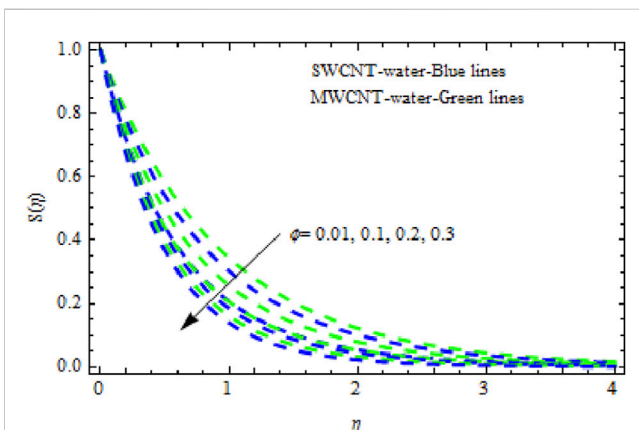


FIGURE 5 Impact of  $\phi$  on  $S(\eta)$ .

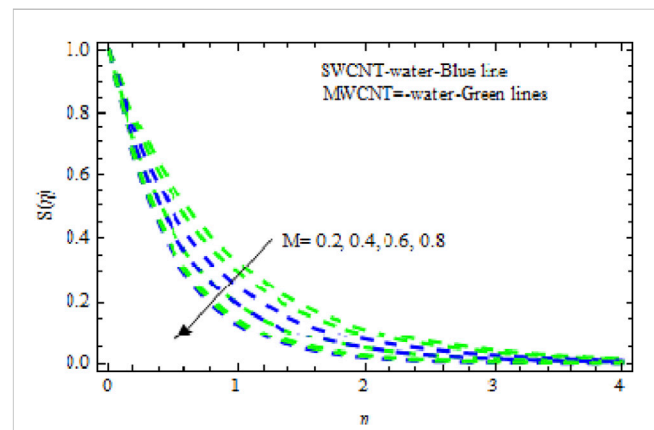


FIGURE 8 Impact of  $M$  on  $S(\eta)$ .

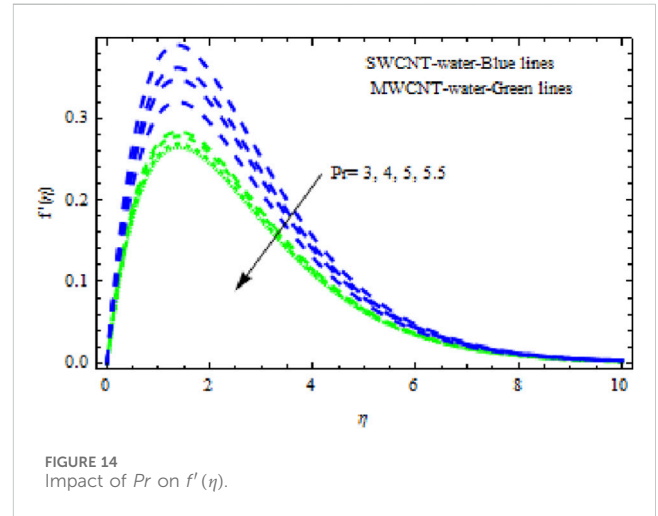
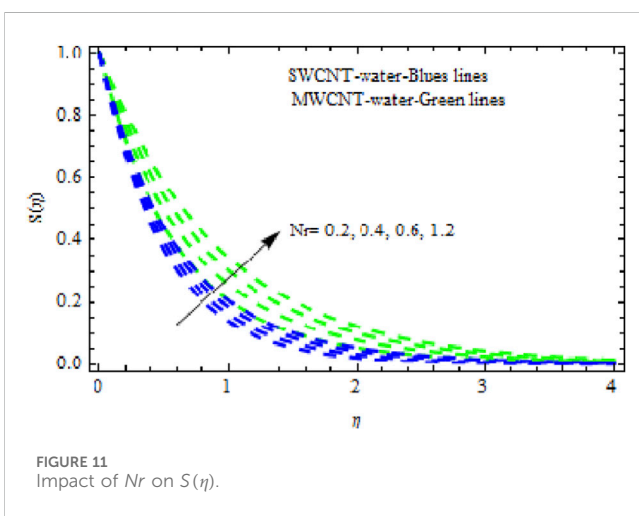
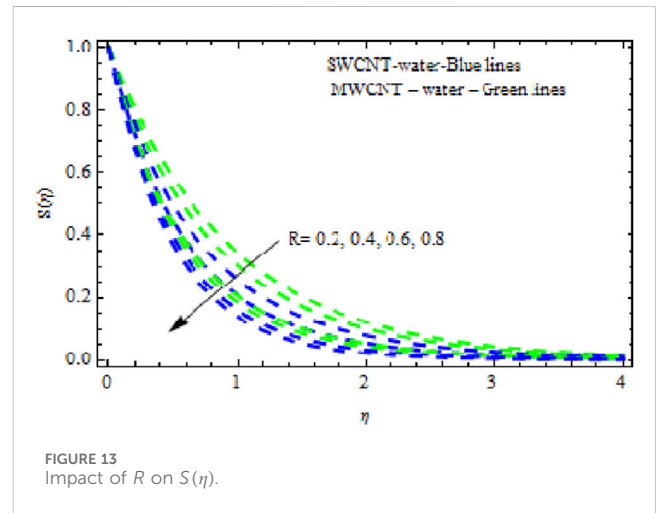
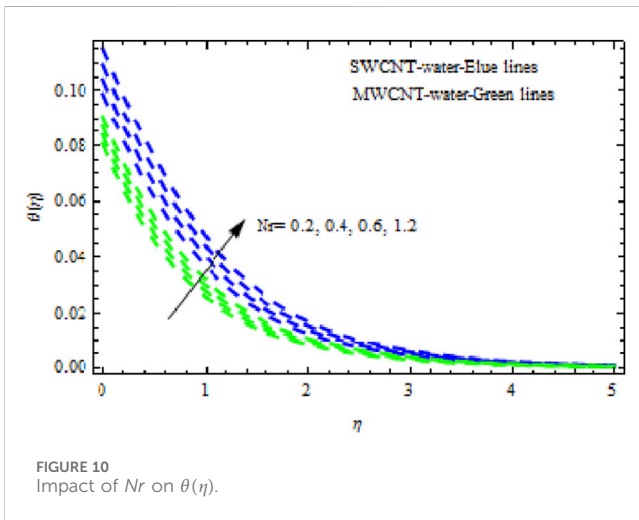
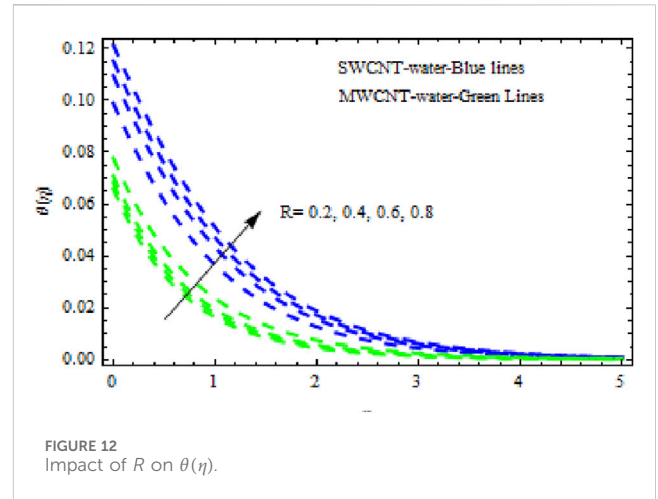
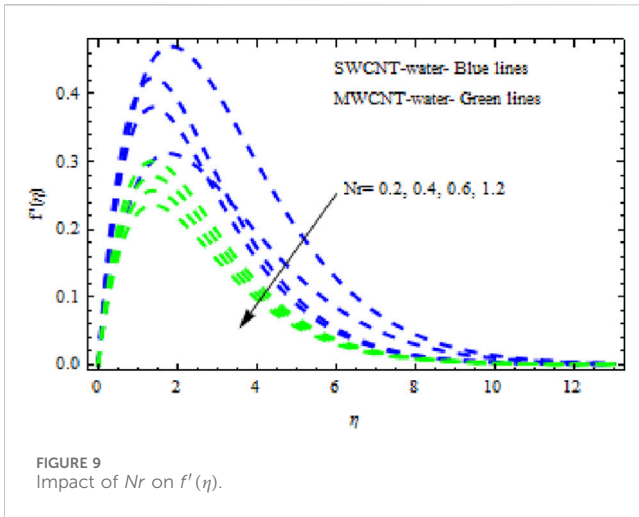
with boundary conditions:

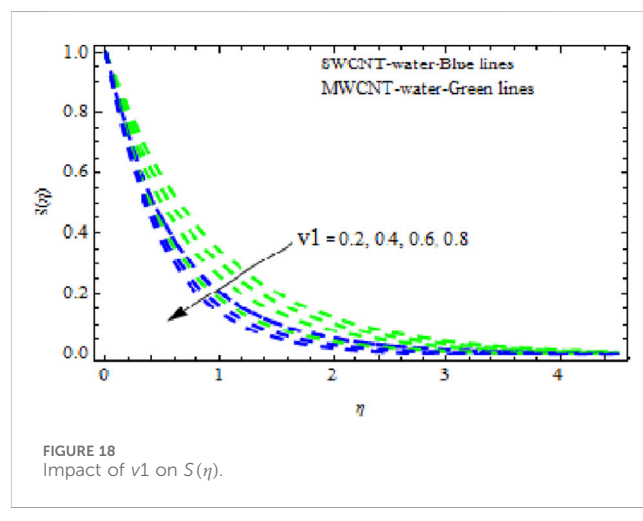
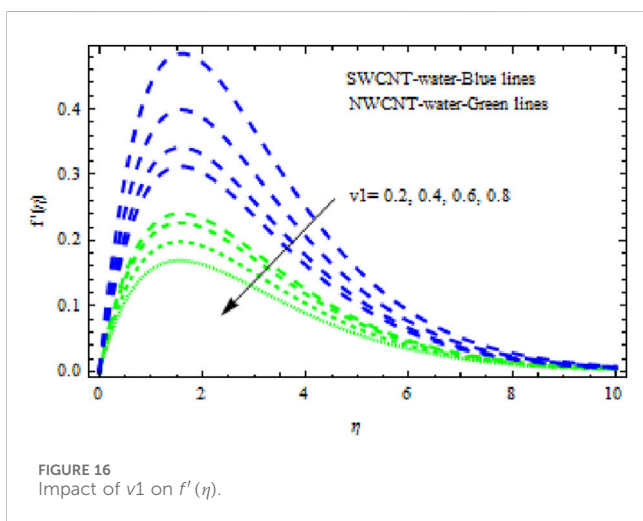
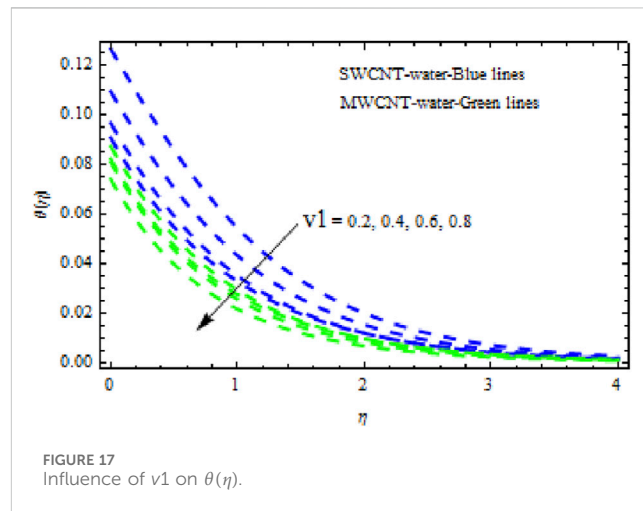
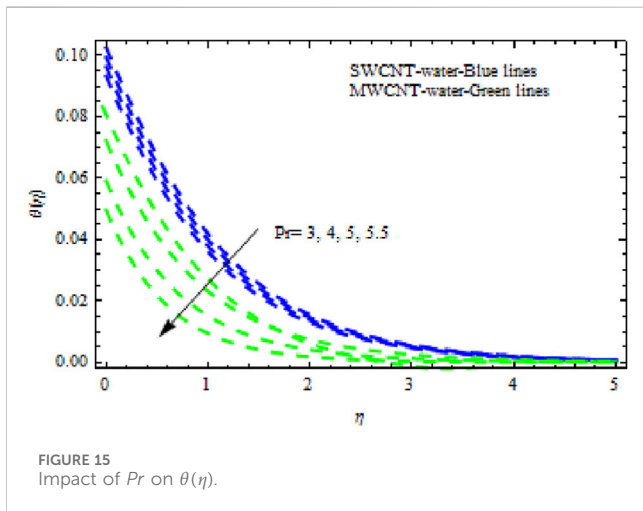
$$u = 0, v = V_1(x), -k_{nf} \frac{\partial T}{\partial y} = h_f(T_f - T), \phi = \phi_w \text{ at } y = 0, \quad (20)$$

$$u \rightarrow 0, T \rightarrow T_\infty, \phi \rightarrow \phi_\infty \text{ at } y \rightarrow \infty. \quad (21)$$

The new similarity transformation is defined by introducing new parameter  $\tau$  :

$$\eta = \frac{y}{x} Ra_x^{\frac{1}{4}}, f(\eta, \tau) = \frac{\psi}{\alpha Ra_x^{\frac{3}{4}}}, \theta(\eta, \tau) = \frac{T - T_\infty}{T_w - T_\infty}, S(\eta, \tau) = \frac{\phi - \phi_\infty}{\phi_w - \phi_\infty}, \tau = ct. \quad (22)$$





Using Equation 22 in Equations 17–21, we obtain

$$\frac{\partial^3 f}{\partial \eta^3} + \frac{A_1}{Pr} \left[ \frac{3}{4} f \frac{\partial^2 f}{\partial \eta^2} - \frac{1}{2} \left( \frac{\partial f}{\partial \eta} \right)^2 \right] - k_1 \frac{\partial f}{\partial \eta} - \frac{\partial^2 f}{\partial \eta \partial \tau} - \frac{A_1}{A_2} M \frac{\partial f}{\partial \eta} + A_1 [\theta - NrS] + \tau \left[ \frac{\partial f}{\partial \tau} \frac{\partial^2 f}{\partial \eta^2} - \frac{\partial f}{\partial \eta} \frac{\partial^2 f}{\partial \eta \partial \tau} \right] = 0, \quad (23)$$

$$(1 + R) \frac{\partial^2 \theta}{\partial \eta^2} + \frac{3}{4} A_3 A_4 f \frac{\partial \theta}{\partial \eta} - \frac{3}{4} A_3 A_4 \left[ \frac{\partial f}{\partial \tau} \frac{\partial \theta}{\partial \eta} - \frac{\partial f}{\partial \eta} \frac{\partial \theta}{\partial \tau} + \frac{\partial \theta}{\partial \tau} \right] = 0, \quad (24)$$

$$\frac{\partial^2 S}{\partial \eta^2} + \frac{3}{4} Sc f \frac{\partial S}{\partial \eta} - CrS + \frac{\partial S}{\partial \tau} = 0. \quad (25)$$

The corresponding boundary constraints are

$$f(0, \tau) = V_0, \frac{\partial f}{\partial \eta}(0, \tau) = 0, \frac{\partial \theta}{\partial \eta}(0, \tau) = -A_4 B_1 (1 - \theta(0, \tau)), S(0, \tau) = 1, \text{ as } \eta = 0, \quad (26)$$

$$\frac{\partial f}{\partial \eta}(\eta, \tau) \rightarrow 0, \theta(\eta, \tau) \rightarrow 0, S(\eta, \tau) \rightarrow 0 \text{ as } \eta \rightarrow \infty.$$

The stability explanation is attained by the steady movement  $f(\eta) = f_0(\eta)$ ,  $\theta(\eta) = \theta_0(\eta)$ , and  $S(\eta) = S_0(\eta)$  by expressing the following relations (Merkin, 1986; Weidman et al., 2006):

$$f(\eta, \tau) = f_0(\eta) + e^{-\gamma \tau} J(\eta, \tau), \theta(\eta, \tau) = \theta_0(\eta) + e^{-\gamma \tau} F(\eta, \tau), S(\eta) = S_0(\eta) + e^{-\gamma \tau} G(\eta, \tau). \quad (27)$$

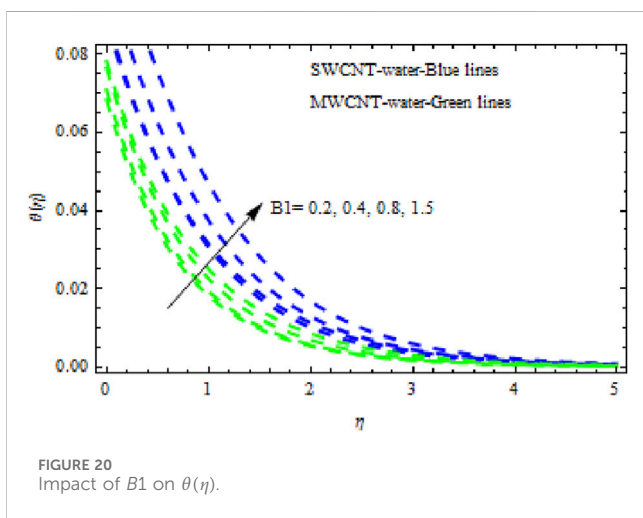
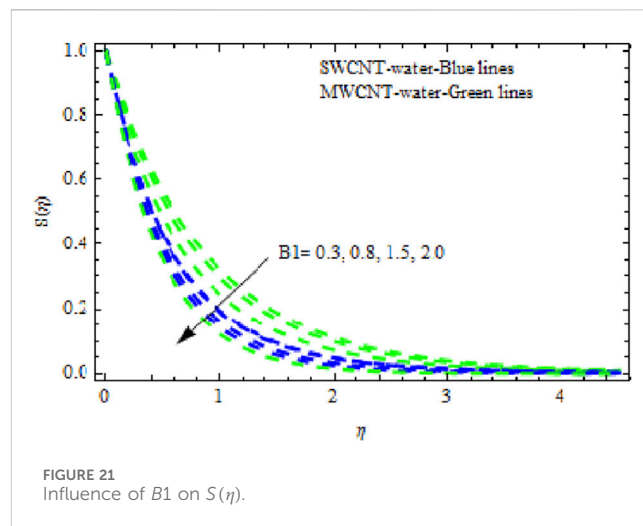
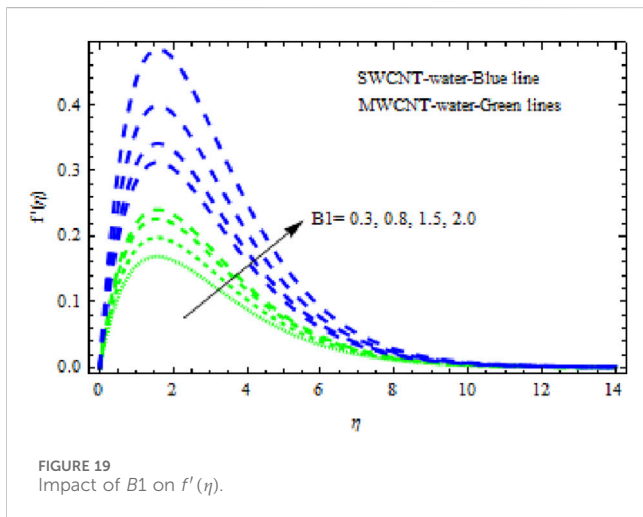
Here,  $\gamma$  is an undetermined eigenvalue and  $J(\eta, \tau)$ ,  $\theta(\eta, \tau)$ , and  $S(\eta, \tau)$  are relatively smaller than  $f_0(\eta)$ ,  $\theta_0(\eta)$ , and  $S_0(\eta)$ .

Using Equation 27 and Equations 23–26, we obtain

$$\frac{\partial^3 J}{\partial \eta^3} + \frac{A_1}{Pr} \left[ \frac{3}{4} f_0 \frac{\partial^2 J}{\partial \eta^2} + f_0' J - f_0' f_0'' \right] - k_1 \frac{\partial J}{\partial \eta} + \frac{\partial^2 J}{\partial \eta \partial \tau} - \frac{A_1}{A_2} M \frac{\partial J}{\partial \eta} + A_1 [F - NrG] + \gamma \left[ \gamma f_0' \frac{\partial J}{\partial \tau} + \frac{\partial J}{\partial \tau} \frac{\partial^2 J}{\partial \eta^2} + f_0' \frac{\partial^2 J}{\partial \eta^2} - f_0' \frac{\partial^2 J}{\partial \eta \partial \tau} \right] = 0, \quad (28)$$

$$(1 + R) \frac{\partial^2 F}{\partial \eta^2} + \frac{3}{4} A_3 A_4 \left( f_0 \frac{\partial F}{\partial \eta} - \theta_0' J \right) - \frac{3}{4} A_3 A_4 \left[ \gamma \theta_0' J + \theta_0 \frac{\partial J}{\partial \tau} - \gamma F f_0 - f_0 \frac{\partial F}{\partial \tau} - \gamma F + \frac{\partial F}{\partial \tau} \right] = 0, \quad (29)$$





$$(1 + R)F_0'' + \frac{3}{4}A_3A_4(f_0F_0' - \theta_0J_0) - \frac{3}{4}A_3A_4[\gamma\theta_0'J_0 - \gamma F_0f_0' - \gamma F_0] = 0, \tag{33}$$

$$G_0'' + \frac{3}{4}Sc(f_0G_0' + S_0J_0) - CrG_0 - \gamma G_0 = 0. \tag{34}$$

The corresponding boundary constraints are

$$\begin{aligned} J_0(0, \tau) = V1, J_0'(0, \tau) = 0, F_0'(0, \tau) = -A_4B1(1 - F_0(0, \tau)), \\ G_0(0, \tau) = 1, J_0'(\eta, \tau) \rightarrow 0, F_0'(\eta, \tau) \rightarrow 0, G_0(\eta, \tau) \rightarrow 0, \text{ as } \eta \rightarrow \infty. \end{aligned} \tag{35}$$

## 5 Results and discussion

This study aims to investigate the impact of single-walled (SWCNTs) and multi-walled (MWCNTs) carbon nanotubes with convective fluid (water) over a perpendicular cone beneath the influences of chemical species, magnetism, thermal radiation, and drenched permeable media. The impact of heat is also examined. Constructed on the flow norms, the fundamental flow characteristics are modeled in terms of partial differential equations (PDEs). Using the appropriate transformation, the PDEs are denaturalized in terms of conventional derivatives (ordinary differential equations) and then solved via RK4 in MATLAB.

The mathematical framework given in Equations 10–13 with Equation 14 presented multiple solutions on behalf of some evolving constraints. Figure 2A demonstrates the sensations of double solutions—reliable (first solution) and unreliable (second solution). Consequently, an immovability examination is executed to determine a reliable solution. Equation 35, as well as linearized Equations 32–34, were numerically solved using RK4 MATLAB software. Figure 2A shows the lowest eigenvalues  $\gamma$  versus V1 when  $\phi = 0.01$ . Subsequently, the suction parameter neared its critical value, and the values of  $\gamma$  propagated nearer to zero in both (first and second) solutions. We suggest that the first solution is stable whereas the second is unreliably constructed on the earlier exploration. This methodology is vital for finding a reliable solution whenever

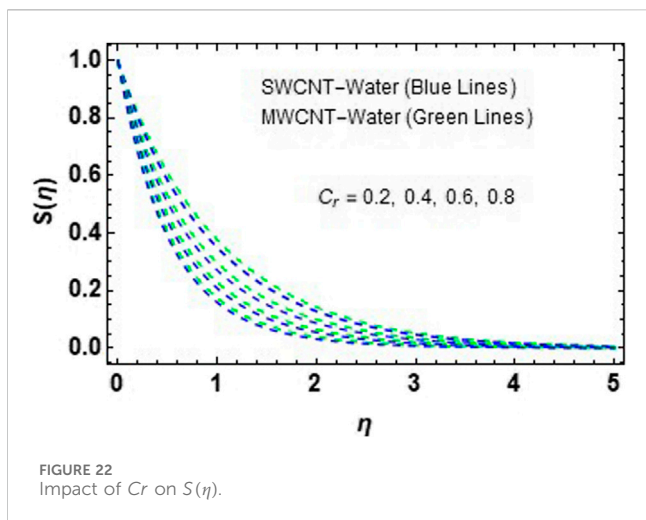
$$\frac{\partial^2 G}{\partial \eta^2} + \frac{3}{4}Sc \left( f_0 \frac{\partial G}{\partial \eta} + S_0 J \right) - CrG - \gamma G + \frac{\partial G}{\partial \tau} = 0. \tag{30}$$

The corresponding boundary constraints are

$$\begin{aligned} J(0, \tau) = V_0, \frac{\partial J}{\partial \eta}(0, \tau) = 0, \frac{\partial F}{\partial \eta}(0, \tau) = -A_4B1(1 - F(0, \tau)), \\ G(0, \tau) = 1, \frac{\partial J}{\partial \eta}(\eta, \tau) \rightarrow 0, F(\eta, \tau) \rightarrow 0, G(\eta, \tau) \rightarrow 0. \text{ as } \eta \rightarrow \infty. \end{aligned} \tag{31}$$

The steady state solution for  $J(\eta) = J_0(\eta)$ ,  $F(\eta) = F_0(\eta)$ , and  $G(\eta) = G_0(\eta)$  for stability analysis is obtained by setting  $\tau = 0$  for the system Equations 11–14. Therefore,  $f(\eta) = f_0(\eta)$ ,  $\theta(\eta) = \theta_0(\eta)$ , and  $S(\eta) = S_0(\eta)$  in system Equations 28–31 signify the initial growth or decay of the solution given by Equation 27. Consequently, the linear eigenvalue problem is obtained thus:

$$\begin{aligned} J_0''' + \frac{A_1}{Pr} \left[ \frac{3}{4}f_0J_0'' + f_0''J - f_0'f_0'' \right] - k1J_0' - \frac{A_1}{A_2}MJ_0' + A_1[F_0 - NrG_0] \\ + \gamma f_0'J_0'' = 0, \end{aligned} \tag{32}$$



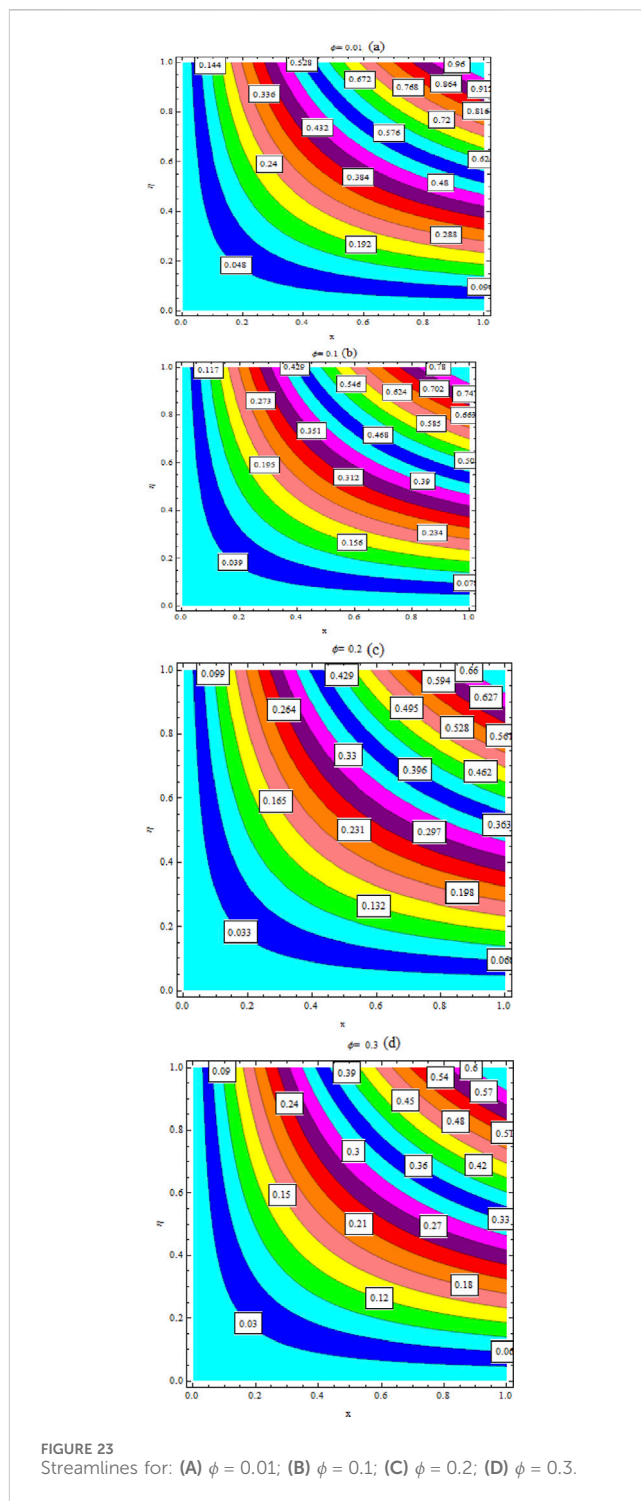
multiple solutions occur, permitting reliable movement-behavior extrapolation.

Figures 2B and C confirm the effects of the volume fraction parameter (VFP) versus suction factor  $\nu_1$  on local skin friction (LSF) and the Nusselt number (NN). In this analysis, duality is observed for the given values  $\nu_1$ . In the case of  $\phi = 0.01$ , solutions are guaranteed to occur for  $\nu_1 c > 1.53271$ , but when  $\phi =$  grows to 0.1 and 0.2 and  $\nu_1 c > 1.51017$  and 1.49824, respectively, the range of suction expands. Additionally, it should be noted that increasing VFP enhances from 0.01 to 0.03, improving both LSF and the NN. Additionally, the values of LSF and the NN for the first solution rise when the suction parameter  $\nu_1$  rises, but the reverse occurs for the second solution.

The impact of radiation and volume fraction parameters on the Sherwood number and LSF is depicted in Figures 2D and E, respectively, along both suction and injection parameters. It is apparent that dual solutions occurred for both the Sherwood number and LSF. However, no solution exists for  $\nu_1 < \nu_{1c}$  (critical point), demonstrating that the boundary layer splits from the cone surface and violates the rules of the boundary layer model. Additionally,  $\nu_{1c}$  is the point of contact that combines the reliable and unreliable solutions. In Figure 2D, the Sherwood number is enhanced in the first and second solutions with increasing radiation parameter when  $\nu_1 > 0$  and declines when  $\nu_1 < 0$ . Figure 2E shows that LSF increases in both the first and second solutions for  $\nu_1 > 0$  and declines for  $\nu_1 < 0$  with growing values of VFP.

We found that the VFP increased the NN in both the first and second solutions (Figure 2F). It is significant that increasing the nanoparticles' VFP enhances heat transportation efficiency. The influence of the Biot number on the NN is demonstrated in Figure 2G. Here, in both first and second solution, the NN increases with a higher Biot number.

The distributions of velocity, temperature, and concentration of nanofluid (NF) (water base), including SWCNTs and MWCNTs, for different values of VFP are shown in Figures 3–5. In both cases, the velocity outlines decreased as VFP increased. It is important to note that for MWCNTs, the velocity of the fluid is significantly degraded in



comparison to the SWCNT-water-based NFs. As VFP increases, the humidity and concentration profiles of both NFs slow. We also found that MWCNTs demonstrate greater thermal boundary layer thickness (TBLT) retardation than SWCNTs. Nevertheless, SWCNT NF experiences a significantly greater decrease in solutal boundary layer width than MWCNT NF. The impact of magnetic factor ( $M$ ) is portrayed in Figures 6–8. Figure 6 shows that for both SWCNT and MWCNT NF, the velocity patterns are impeded across the boundary layer with

increasing values of magnetic factor ( $M$ ). Because the Lorentz effect, due to applied magnetic field, serves as a resistive force, boundary layer movement decreases everywhere in the flow. With greater values of ( $M$ ), the depth of the hydrodynamic boundary layer in MWCNT NF (water as base fluid) declines more quickly than SWCNT-NF (water as base fluid). **Figure 7** displays that as the magnitude of ( $M$ ) grows, the temperature curves of both liquids rise but rises significantly in SWCNT NF compared to MWCNT NF. **Figure 8** shows that when ( $M$ ) increases, the concentration curves move in the opposite direction of the temperature curves. In **Figures 9–11**, we see how varying the Buoyancy ratio parameter ( $Nr$ ) affects the flow characteristics. As illustrated in **Figure 9**, both NFs experience a significant slowing in mobility with increasing levels of ( $Nr$ ). It was detected that with larger values of ( $Nr$ ), the temperature curves for the two NFs become more complex. This is because the thermal boundary layer thickness rises with growing ( $Nr$ ) (**Figure 10**). Likewise, the concentration characteristics rise with increasing ( $Nr$ ). **Figure 11** shows that the concentration patterns of MWCNT NFs rise more highly than those of SWCNT NFs. **Figures 12, 13** show the temperature and concentration variations in the SWCNT and MWCNT NFs for different variations of radiation parameter ( $R$ ). It is observed for both NFs that the thermal-boundary depth is enriched when  $R$  increases. This is because when  $R$  is enhanced, the Rosseland radiated absorptive  $k$  is too. This occurs more highly due to the rate of heating being submerged, denoted by  $\partial q_r/\partial y$ . Enhanced radiative heat transmission promotes the expansion of the thermal boundary layer. However, when  $R$  grows, the concentration profiles become less robust in the fluid area. This slowdown in the thickness of the solutal boundary layer is thought to be more pronounced in MWCNT NF than in SWCNT NF. The consequence of the Prandtl number ( $Pr$ ) on fluid flow and heat curves is seen in **Figures 14, 15**. As shown in **Figure 14**, MWCNT NF experiences a greater decrease in velocity distributions over the entire boundary layer regime than SWCNT NF when the value of  $Pr$  increases. In addition, higher concentrations of  $Pr$  in both NFs lead to lower temperature distributions. Physically, a higher Prandtl number indicating lower thermal diffusivity signifies the smallest heat diffusion rate in the fluid. Consequently, as shown in **Figure 15**, heat and the thermal boundary layer decline. Furthermore, deceleration is greater in MWCNT NF than in SWCNT NF. In **Figures 16–18**, we see how dimensionless velocity, temperature, and concentration vary with differing suction/injection factors ( $\nu_1$ ). With increasing values of  $\nu_1 (>0)$ , it appears that all of the curves degrade across the boundary layer zone for both NFs. This is because suction removes heated fluid through the boundary layer regime, causing a decrease in the thickness of all boundary layers. Additionally, MWCNT NF exhibits greater degradation in temperature and flow rate than SWCNT NF. The latter, however, exhibits decreasing concentration distributions at a greater rate than MWCNT NF (**Figure 18**). **Figures 19–21** show how the Biot number ( $B1$ ) affects the momentum, temperature, and solute boundary layers for the two NFs. **Figures 19** and **20** show that the flow rate and temperature of the liquid noticeably

increase, and this rise is higher in SWCNT NFs than in MWCNT NFs. Physically, when  $B1$  is augmented, the inner thermal force increases relative to the thermal boundary layer, raising the fluid's heat in the boundary layer regime. However, when  $B1$  values increase in intensity, the concentration profiles of the two NFs decrease (**Figure 21**). For SWCNT NF and MWCNT NFs, the solutal boundary layer is plotted in **Figure 22** with varied values of the chemical reaction factor ( $Cr$ ). It has been noted that MWCNT NFs exhibit significantly more degradation in concentration curves than SWCNT NFs. Streamlines are plotted in **Figures 23A–D**.

## 6 Conclusion

We here examine the heat transfer behavior and chemical interactions on the movement of water-based nanofluids (NFs) including single- (SWCNT) and multiple-walled (MWCNT) carbon nanotubes (CNTs) across an upward cone inserted into a porous material under a convection boundary constraints. The system of ordinary differential equations is numerically solved via RK4. Hydrodynamic, thermal, and solutal boundary layers are studied, and the effects of varying relevant parameters are shown graphically. The present analysis reveals the dual solution for the suction and injection parameter, and stability analysis is performed to confirm which solution is stable. The aim of this study is to analyze SWCNTs and MWCNTs in a vertical cone with stability to established that only the first solution is reliable. A table presentation displays the outcomes of LSF, heat transfer rate, NN, SN, and concentration. It is found that in both nanofluids, the heat transmission rate is a growing function of  $\phi$ . Interestingly, the heat transmission rate is sophisticated in MWCNT water-based NF. The fluid rate diminishes with the growing magnitude of the magnetic factor ( $M$ ) while heat is enhanced with  $M$ . Heat mass transportation increases in both NFs with the augmented values of  $\nu_1 > 0$ . This increase is higher in MWCNT NF. The temperature curves are augmented with the growing values of  $B1$ .

### 6.1 Future suggestions

This model's usefulness is rather limited because it depends solely on a two-dimensional flow arrangement that includes conventional thermal and mass boundary circumstances. Still, the inquiry would be useful for engineering purposes if conducted in three dimensions via the passive control technique and includes a convection heating/melting heat exchange mechanism along with stability assessment.

### Data availability statement

The original contributions presented in the study are included in the article/supplementary material; further inquiries can be directed to the corresponding authors.

## Author contributions

HX: writing–review and editing and writing–original draft. FA: writing–review and editing and methodology. EI: writing–review and editing, supervision, and formal analysis. WK: writing–review and editing and software.

## Funding

The author(s) declare financial support was received for the research, authorship, and/or publication of this article. Researchers Supporting Project number (RSPD2025R1060), King Saud University, Riyadh, Saudi Arabia.

## References

- Abu-Bakr, A. F., Kanagawa, T., and Abu-Nab, A. K. (2022). Analysis of doublet bubble dynamics near a rigid wall in ferrofluid nanofluids. *Case Stud. Therm. Eng.* 34, 102060. doi:10.1016/j.csite.2022.102060
- Akbar, N. S., Akhtar, S., Maraj, E. N., Anqi, A. E., and Homod, R. Z. (2023b). Heat transfer analysis of MHD viscous fluid in a ciliated tube with entropy generation. *Math. Methods Appl. Sci.* 46 (10), 11495–11508. doi:10.1002/mma.7906
- Akbar, N. S., Mehri, A. A., Rafiq, M., Habib, M. B., and Muhammad, T. (2023a). Peristaltic flow analysis of thermal engineering nano model with effective thermal conductivity of different shape nanomaterials assessing variable fluid properties. *Alexandria Eng. J.* 81, 395–404. doi:10.1016/j.aej.2023.09.027
- Akbar, N. S., Rafiq, M., Muhammad, T., and Alghamdi, M. (2024). Electro osmotically interactive biological study of thermally stratified micropolar nanofluid flow for Copper and Silver nanoparticles in a microchannel. *Sci. Rep.* 14 (1), 518. doi:10.1038/s41598-023-51017-z
- Alghamdi, M., Akbar, N. S., Zamir, T., and Muhammad, T. (2024). Double layered combined convective heated flow of Eyring–Powell fluid across an elevated stretched cylinder using intelligent computing approach. *Case Stud. Therm. Eng.* 54, 104009. doi:10.1016/j.csite.2024.104009
- Amrollahi, A., Rashidi, A. M., Lotfi, R., Meibodi, M. E., and Kashefi, K. (2010). Convection heat transfer of functionalized MWNT in aqueous fluids in laminar and turbulent flow at the entrance region. *Int. Commun. Heat. Mass Transf.* 37, 717–723. doi:10.1016/j.icheatmasstransfer.2010.03.003
- Anjum, N., Khan, W. A., Hobiny, A., Azam, M., Waqas, M., and Irfan, M. (2022). Numerical analysis for thermal performance of modified Eyring–Powell nanofluid flow subject to activation energy and bioconvection dynamic. *Case Stud. Therm. Eng.* 39, 102427. doi:10.1016/j.csite.2022.102427
- Azeem Khan, W. (2022). Impact of time-dependent heat and mass transfer phenomenon for magnetized Sutterby nanofluid flow. *Waves random complex media*, 1–15. doi:10.1080/17455030.2022.2140857
- Buongiorno, J. (2006). Convective transport in nanofluids. *Heat. Mass Transf.* 128, 240–250. doi:10.1115/1.2150834
- Chamkha, A. J., and Rashad, A. M. (2014). Unsteady heat and mass transfer by MHD mixed convection flow from a rotating vertical cone with chemical reaction and Soret and Dufour effects. *Can. J. Chem. Eng.* 92, 758–767. doi:10.1002/cjce.21894
- Choi, S. U. S., and Eastman, J. A. (1995a). Enhancing thermal conductivity of fluids with nanoparticles, San Francisco. *ASME Int. Mech. Eng. Congr. Expo.*, 12–17.
- Choi, S. U. S., and Eastman, J. A. (1995b). *Enhancing thermal conductivity of fluid with nanofluids*.
- Hayat, T., Hussain, Z., Alsaedi, A., and Hobiny, A. (2017a). Computational analysis for velocity slip and diffusion species with carbon nanotubes. *Results Phys.* 7, 3049–3058. doi:10.1016/j.rinp.2017.07.070
- Hayat, T., Hussain, Z., Farooq, M., and Alsaedi, A. (2017b). Homogeneous and heterogeneous reactions effects in flow with Joule heating and viscous dissipation. *J. Mech.* 33 (1), 77–86. doi:10.1017/jmech.2016.71
- Hayat, T., Qasim, M., and Mesloub, S. (2011). MHD flow and heat transfer over permeable stretching sheet with slip conditions. *Int. J. Numer. Methods Fluids* 66, 963–975. doi:10.1002/flid.2294
- Hayat, T., Shah, F., Hussain, Z., and Al-Saedi, A. (2019). Darcy Forchheimer flow of Jeffrey nanofluid with heat generation/absorption and melting heat transfer. *Therm. Sci.* 23, 3833–3842. doi:10.2298/tsci171222314h
- HinanS, H. T., Asghar, S., and Hendi, A. A. (2012). Influence of compliant walls on peristaltic motion with heat/mass transfer and chemical reaction. *Int. J. Heat. Mass Transf.* 55, 3386–3394. doi:10.1016/j.ijheatmasstransfer.2012.02.074
- Hussain, Z., Bashir, Z., and Anwar, M. S. (2022). Analysis of nanofluid flow subject to velocity slip and Joule heating over a nonlinear stretching Riga plate with varying thickness. *Waves Random Complex Media*, 1–17. doi:10.1080/17455030.2022.2124468
- Khan, A., Zaman, G., and Rahman, G. (2015). Hydromagnetic flow near a non-uniform accelerating plate in the presence of magnetic field through porous medium. *J. Porous Media* 18, 801–809.
- Khan, W. A. (2023a). Significance of magnetized Williamson nanofluid flow for ferromagnetic nanoparticles. *Waves Random Complex Media*, 1–20. doi:10.1080/17455030.2023.2207390
- Khan, W. A. (2023b). Dynamics of gyrotactic microorganisms for modified Eyring–Powell nanofluid flow with bioconvection and nonlinear radiation aspects. *Waves Random Complex Media*, 1–11. doi:10.1080/17455030.2023.2168086
- Khan, W. A., Waqas, M., Chammam, W., Asghar, Z., Nisar, U. A., and Abbas, S. Z. (2020a). Evaluating the characteristics of magnetic dipole for shear-thinning Williamson nanofluid with thermal radiation. *Comput. Methods Programs Biomed.* 191, 105396. doi:10.1016/j.cmpb.2020.105396
- Khan, W. A., Waqas, M., Kadry, S., Asghar, Z., Abbas, S. Z., and Irfan, M. (2020b). On the evaluation of stratification-based entropy optimized hydromagnetic flow featuring dissipation aspect and Robin conditions. *Comput. Methods Programs Biomed.* 190, 105347. doi:10.1016/j.cmpb.2020.105347
- Maraj, E. N., Shah, S. I., Akbar, N. S., and Muhammad, T. (2023). Thermally progressive Particle–Cu/Blood peristaltic transport with mass transfer in a Non-Uniform Wavy Channel: closed-form exact solutions. *Alexandria Eng. J.* 74, 453–466. doi:10.1016/j.aej.2023.05.056
- Memon, A. A., Murtaza, S., Memon, M. A., Bhatti, K., Haque, M., and Ali, M. R. (2022). Simulation of thermal decomposition of Calcium Oxide in water with different activation energy and the high Reynolds number. *Complexity* 2022, 3877475. doi:10.1155/2022/3877475
- Merkin, J. H. (1986). On dual solutions occurring in mixed convection in a porous medium. *J. Eng. Math.* 20, 171–179. doi:10.1007/bf00042775
- Miroshnichenko, I. V., Sheremet, M. A., Oztop, H. F., and Al-Salem, K. (2016). MHD natural convection in a partially open trapezoidal cavity filled with a nanofluid. *Int. J. Mech. Sci.* 119, 294–302. doi:10.1016/j.ijmecsci.2016.11.001
- Oztop, H. F., Sakhrieh, A., Abu-Nada, E., and Al-Salem, K. (2017). Mixed convection of MHD flow in nanofluid filled and partially heated wavy walled lid-driven enclosure. *Int. Commun. Heat. Mass Transf.* 86, 42–51. doi:10.1016/j.icheatmasstransfer.2017.05.011
- Pakdamana, M. F., Akhavan-Behabadi, M. A., and Razi, P. (2012). An experimental investigation on thermo-physical properties and overall performance of MWCNT/heat transfer oil nanofluid flow inside vertical helically coiled tubes. *Exp. Therm. Fluid Sci.* 40, 103–111. doi:10.1016/j.expthermflusc.2012.02.005
- Rashmi, W., Ismail, A. F., Sopyan, I., Jameel, A. T., Yusof, F., Khalid, M., et al. (2011). Stability and thermal conductivity enhancement of carbon nanotube nanofluid using gum Arabic Arabic. *J. Exp. Nanosci.* 6, 567–579. doi:10.1080/17458080.2010.487229
- Selimfendigil, F., and Oztop, H. F. (2016a). Conjugate natural convection in a cavity with a conductive partition and filled with different nanofluids on different sides of the partition. *J. Mol. Liq.* 216, 67–77. doi:10.1016/j.molliq.2015.12.102

## Conflict of interest

The authors declare that the research was conducted in the absence of any commercial or financial relationships that could be construed as a potential conflict of interest.

## Publisher's note

All claims expressed in this article are solely those of the authors and do not necessarily represent those of their affiliated organizations, or those of the publisher, the editors, and the reviewers. Any product that may be evaluated in this article, or claim that may be made by its manufacturer, is not guaranteed or endorsed by the publisher.

- Selimefendigil, F., and Oztop, H. F. (2016b). Analysis of MHD mixed convection in a flexible walled and nanofluids filled lid-driven cavity with volumetric heat generation. *Int. J. Mech. Sci.* 118, 113–124. doi:10.1016/j.ijmecsci.2016.09.011
- Sudarsana Reddy, P., and Chamkha, A. J. (2016b). Soret and Dufour effects on MHD convective flow of Al<sub>2</sub>O<sub>3</sub>-water and TiO<sub>2</sub>-water nanofluids past a stretching sheet in porous media with heat generation/absorption with heat generation/absorption. *Adv. Powder Technol.* 27, 1207–1218. doi:10.1016/j.apt.2016.04.005
- Sudarsana Reddy, P., and Chamkha, A. J. (2016b). Influence of size, shape, type of nanoparticles, type and temperature of the base fluid on natural convection MHD of nanofluids type and temperature of the base fluid on natural convection MHD of nanofluids. *Alex. Eng. J.* 55, 331–341. doi:10.1016/j.aej.2016.01.027
- Tasawar, H., Rashid, M., Maria, I., and Ahmed, A. (2015). Magneto hydrodynamic (MHD) flow of Cu-water nanofluid due to a rotating disk with partial slip. *AIP Adv.* 5, 067169. doi:10.1063/1.4923380
- Wang, J., Zhu, J., Zhang, X., and Chen, Y. (2013). Heat transfer and pressure drop of nanofluids containing carbon nanotubes in laminar flows. *Exp. Therm. Fluid Sci.* 44, 716–721. doi:10.1016/j.expthermflusci.2012.09.013
- Waqas, M., Khan, W. A., Pasha, A. A., Islam, N., and Rahman, M. M. (2022). Dynamics of bioconvective Casson nanoliquid from a moving surface capturing gyrotactic microorganisms, magnetohydrodynamics and stratifications. *Therm. Sci. Eng. Prog.* 36, 101492. doi:10.1016/j.tsep.2022.101492
- Weidman, P. D., Kubitschek, D. G., and Davis, A. (2006). The effect of transpiration on self-similar boundary layer flow over moving surfaces. *Int. J. Eng. Sci.* 44, 730–737. doi:10.1016/j.ijengsci.2006.04.005
- Xuan, Y. M., and Li, Q. (2000). Heat transfer enhancement of nanofluids. *Int. J. Heat. Fluid fl* 21, 58–64. doi:10.1016/S0142-727X(99)00067-3
- Xue, Q. (2005). Model for thermal conductivity of carbon nanotube-based composites. *Phys. B Condens Matter* 368, 302–307. doi:10.1016/j.physb.2005.07.024